Dynamic instability transitions in one-dimensional driven diffusive flow with nonlocal hopping

Meesoon Ha,[1,2] Hyunggyu Park,[2] and Marcel den Nijs[3]
[1]*Department of Physics, Chonbuk National University, Jeonju 561-756, Korea*
[2]*School of Physics, Korea Institute for Advanced Study, Seoul 130-722, Korea*
[3]*Department of Physics, University of Washington, Seattle, Washington 98195, USA*
(Received 24 March 2007; published 29 June 2007)

One-dimensional directed driven stochastic flow with competing nonlocal and local hopping events has an instability threshold from a populated phase into an empty-road (ER) phase. We implement this in the context of the asymmetric exclusion process. The nonlocal skids promote strong clustering in the stationary populated phase. Such clusters drive the dynamic phase transition and determine its scaling properties. We numerically establish that the instability transition into the ER phase is second order in the regime where the entry point reservoir controls the current and first order in the regime where the bulk is in control. The first-order transition originates from a turnabout of the cluster drift velocity. At the critical line, the current remains analytic, the road density vanishes linearly, and fluctuations scale as uncorrelated noise. A self-consistent cluster dynamics analysis explains why these scaling properties remain that simple.

DOI: 10.1103/PhysRevE.75.061131 PACS number(s): 64.60.Cn, 05.70.Ln, 05.40.−a, 02.50.Ga

I. INTRODUCTION

Driven stochastic diffusive flow of particles in narrow channels is widely used as a prototype process to study dynamic scaling. The central interests in such processes reside with the structure of nonequilibrium stationary (NES) states, the dynamical pathways to those NES states, and the scaling properties of dynamic phase transitions. Driven stochastic processes often undergo dynamic phase transitions inside their NES states as a function of control parameters. This is true even in one dimension where equilibrium phase transitions are forbidden. One-dimensional (1D) processes serve thus as ideal platforms to unearth novel general principles affecting the dynamic scaling properties and the structure of NES state distributions. The maximum entropy principle familiar from thermal equilibrium, leading to the Gibbs distribution, does not apply to driven systems. We need to formulate new principles, if possible, to predict the structures of NES states [1,2]. Such principles can emerge from the study of a wide array of specific processes, in particular using numerical simulations and/or exact solutions.

In this paper, we address how clustering induced by nonlocal stick-slip events affects 1D driven stochastic diffusive flow. Our model is a generalization of the conventional asymmetric exclusion process (ASEP) [3,4]. We allow nonlocal forward hopping events across empty stretches of road, which introduces an instability toward an "empty-road" (ER) phase.

Clustering and queuing have been studied recently in different generalizations of ASEP. In the conventional ASEP, particles hop stochastically in a preferred direction along a loop, without being able to pass each other and with the occupation of each site limited to one. That ASEP stationary state is surprisingly trivial, completely disordered. However, it is very sensitive to defects and boundary conditions. The sensitivity to reservoirs in open boundary type setups was discovered first. In that setup the stationary state is known exactly by the so-called matrix product ansatz [2,4]. The two reservoirs at the edges of the channel compete with the bulk for control over the bulk density ρ and the average flow rate. This gives rise to phase transitions between bulk- and reservoir-controlled phases. The latter can be viewed as elementary forms of queuing (traffic jams). The density profiles near reservoirs have exponential or power-law tails. The scaling properties remain rather simple and are qualitatively understood from the fact that the ASEP bulk stationary state is fully uncorrelated, while fluctuations spread as $l \sim t^{1/z}$ with $z=3/2$, and travel with group velocity $v_g=1-2\rho$ (see e.g., Ref. [5]).

Introducing bulk impurities to the ASEP, e.g., a single slow bond in the bulk, represents the next level of complexity in queuing. Such a single static defect creates more intricate types of jamming than edges, because, unlike reservoirs, information and correlations can travel across the obstacle. Recently we demonstrated that the scaling properties of the slow-bond queuing transition are nontrivial. We established the existence of an intermediate phase with a pure power-law-shaped queue, and showed that the transition into the macroscopic jammed phase does not take place until a finite strength of the obstruction [6,7].

A next step in the queuing and clustering saga is to allow such impurities to be mobile and participate in the dynamics. Macroscopic clustering represents jamming. For example, in the two-species process by Arndt *et al.* [8], particles of opposite charge hop in opposite directions and the passing of species creates jamming. The stationary states of such processes show strong clustering. The possibility of phase separation into macroscopic clustered states is discussed at length in the literature both numerically [9] and analytically [10], as well as the link to the zero-range process (ZRP) [11].

In this paper, we study queuing caused by a different mechanism. In our generalization of the ASEP, clustering is induced by nonlocal hopping events. A particle can jump with probability $1-p$ to the nearest-neighbor site (if empty) or with probability p all the way forward to the site immediately behind the particle in front of it. We use open boundary conditions with reservoirs at both edges. Starting off as uniform at $p=0$, the stationary state becomes increasingly lumpy with well-defined clusters as p increases. Then, at a

critical value p_c, this clustered liquid becomes unstable and the road empties out. The location and the nature of this phase transition are our main concerns. The transition turns out to be discontinuous or critical. Clustering and coarsening prove to be essential in explaining both.

Clustering is quite common in driven stochastic flow. It appeared, for example, in the two-species-type process of Arndt *et al.* [8]. Those clusters were successfully described by the ZRP [11], which have zero drift. In our process, the nonlocality induces clustering with nonzero drift. More importantly, that aspect induces first- and second-order phase transitions, and the scaling properties of those are governed by the clustering.

This process and its phase transitions also relate to various viscous and/or dissipative stick-slip-type phenomena, where the particle number is the only locally conserved variable. Potential applications include traffic and/or granular flow [12], the motion of stick and flow in sandpiles [13], phase separation in steady sedimentation of colloidal crystals [14,15], electronic and/or molecular transport in nanoscale systems [16], phase ordering in rough films [17], the motion of molecular motors driven by ATP [18], the motion of a depinned flux lattice in a current-carrying superconductor [19], and so on. Nonlocal hopping can be used to mimic the dynamic features associated with, e.g., the competition between maximum and minimum speed or drift in traffic or granular flow, inertia of falling grains inside avalanche processes in sandpiles, and the role of gravity in dynamic and static sedimentation.

This paper is organized as follows. In Sec. II, we present numerical results for the phase diagram, clustering, and nature of the phase transitions. In Sec. III, we set up a self-consistent free cluster analysis, in which the stationary state is described in terms of a collection of freely drifting clusters, i.e., self-organized mesoscopic collective objects that absorb and emit individual particles constantly. The first-order segment of the phase transition line is explained as the result of a turnabout in the drift velocity of those free clusters. The critical segment of the transition line is caused by starvation, and the fluctuations in the density near the entry reservoir become crucial. To describe this, we extend in Sec. IV the self-consistent cluster analysis to the mother cluster, which is the cluster attached to the entry point reservoir. This analysis explains the numerical details of the critical transition presented in Sec. V and discussed in Sec. VI. The paper concludes, in Sec. VII, with a brief summary of the results and some open questions.

Our self-consistent cluster approximations resemble recent zero-range process treatments of clustering phenomena, e.g., in the ASEP with two or more species of particles (driven in opposite directions) [10]. Our approach is both more basic and more general. In those processes the clusters are stationary on average, while ours have a nonzero drift velocity. In the ZRP approach the internal structure of the clusters is ignored, while in our approach the internal density profile is taken into account. Both aspects are essential for the transition into the ER phase. The ZRP can be solved exactly, while our discussion remains more approximate.

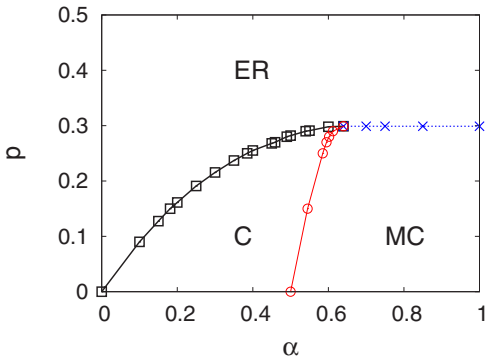

FIG. 1. (Color online) α-p phase diagram from our numerics.

II. PHASE DIAGRAM

Consider a chain of length $1 \leqslant x \leqslant L$ with sites that can only be empty or occupied, $n_x=0,1$. The chain is open, in contact with the entry side reservoir at $x=0$ and the exit side reservoir at $x=L+1$. The updated rule for our process is as follows.

(1) Select a site, $0 \leqslant x \leqslant L$, at random.

(2) If $x \neq 0$ and it is occupied, the particle slides to its nearest-neighbor site $x+1$ (with probability $1-p$) or detaches and jumps all the way to the empty site directly behind the nearest particle in front of it (with probability p).

(3) In case the chain is completely empty in front of the particle, the particle jumps all the way forward into the exit side reservoir.

(4) If the entry side reservoir, $x=0$, is selected and site $x=1$ is empty, a particle jumps onto site $x=1$ with probability α. Nonlocal hopping events from the reservoir are not allowed in our setup.

Figure 1 shows the phase diagram obtained from our Monte Carlo simulations with road lengths up to $L=16\,000$. At $p=0$ the process reduces to the conventional ASEP. There, the stationary state is well known to be in either the input reservoir-controlled phase (C) for $\alpha<\frac{1}{2}$, where the bulk density is set and limited by the influx fugacity α; or the bulk-controlled phase (MC) for $\alpha>\frac{1}{2}$, where the influx rate is no longer the limiting factor and the bulk density is set by maximizing the bulk current.

The C and MC phases persist into $p>0$, but become increasingly clustered (see Fig. 2). Their historical names become quite unfortunate. "MC phase" stands in the conventional ASEP context for "maximal current phase." Control over the current, by either the bulk or the reservoir, is closely linked at $p=0$ with the so-called maximal current principle. The latter has been proposed as a general principle to predict dynamic stationary states. Its success in the conventional ASEP is closely tied to the stationary state being uniform and clusterless, and well approximated by mean-field (MF) theory. The maximal current principle arose naturally as a reformulation of the MF iteration process. Its generalization to strongly clustered states remains unclear, and this issue plays an important role in the discussion below.

"Bulk in control" and "reservoir controlled" would be better names for the two phases in Fig. 2, but we avoid confu-

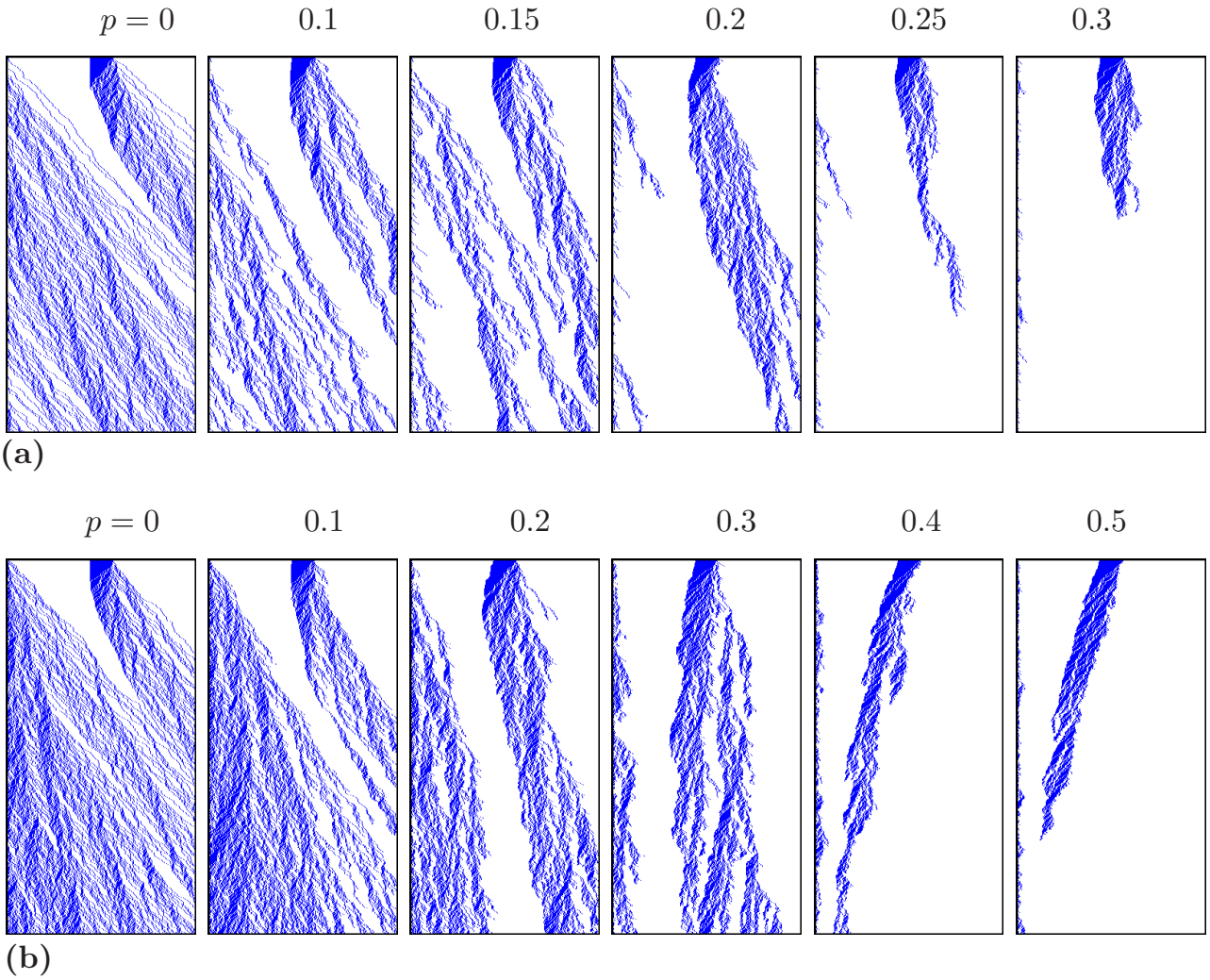

FIG. 2. (Color online) Spatiotemporal density profiles for $L=256$ ($1\leqslant x\leqslant$ running horizontally from left to right) up to $t=512$ ($0\leqslant t\leqslant$ running vertically from top to bottom) illustrating clustering in both (a) ($\alpha\simeq 0.25$: $p_c\simeq 0.19$) the C and (b) ($\alpha\simeq 1.0$: $p_c\simeq 0.30$) the MC phase. Initial conditions include one compact free cluster in the middle of the system to show clearly that the drift velocity of the free clusters turns around at $p\simeq 0.3$.

sion by preserving their historical abbreviations MC (the-middle-in-control phase) and C (being-controlled phase). In the C phase, the stationary-state current varies with both p and α, while in the MC phase it varies only with p regardless of boundary conditions, i.e., it is α independent; see Fig. 3. This feature distinguishes the two phases in our numerical analysis.

For strong nonlocal hopping (large p), the stationary state transforms into an empty-road phase. The transition line starts at small α as a critical line, located just below $p=\alpha$. It levels off for increasing α, and changes at the critical end point, at $\alpha=0.64(1)$, into a first-order transition line. The latter is a strictly horizontal line, with $p_c=0.300(2)$ (see Fig. 1). The density of particles ρ_r jumps to zero at the first-order line (see Fig. 4), but the average current remains continuous (see Figs. 3 and 5).

The road is not truly empty in the ER phase. The average bulk density vanishes, but typically a finite cluster of particles "hangs" still from the entry side reservoir near $x=1$, and some isolated clusters and individual particles are traveling through the bulk. Figures 6 and 7 illustrate this. They show the evolution of the probability distribution for finding $N_r=\rho_r L$ particles on the road across the first-order transition, at $\alpha=0.75$, and across the critical line, at $\alpha=0.2$. Note the gradual evolution of the distribution across p_c at $\alpha=0.2$ versus the abrupt change at $\alpha=0.75$.

Consider the average current through a bulk bond between x and $x+1$,

$$\langle J_{x+1/2}\rangle = \langle n_x v_{x+1}\rangle + p\langle v_x v_{x+1}\rangle - pP_0(x+1), \qquad (1)$$

and through the edge bonds

$$\langle J_{1/2}\rangle = \alpha\langle v_1\rangle, \quad \langle J_{L+1/2}\rangle = \langle n_L\rangle + p\langle v_L\rangle - pP_0(L), \qquad (2)$$

where n_x is the occupation operator at site x, and $v_x\equiv 1-n_x$ is the vacancy operator. Equation (1) states that the current through the bulk bond is zero if site $x+1$ is occupied; equal to 1 if site $x+1$ is empty while x is occupied; and equal to p if both sites are empty, provided at least one particle exists on the road somewhere to the left of $x+1$. The latter requires

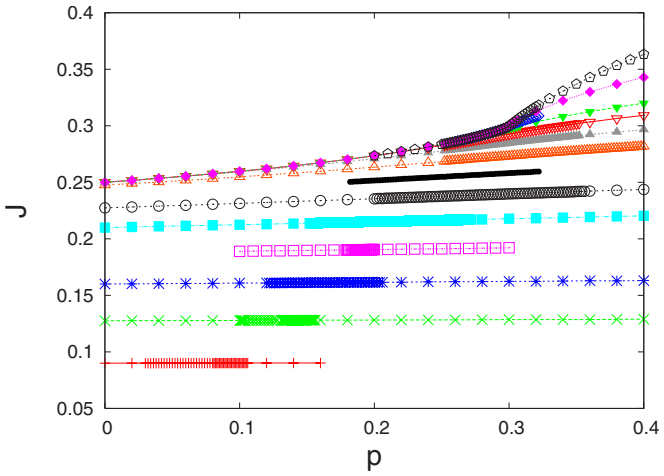

FIG. 3. (Color online) Steady-state current J versus p for $L=8000$ at fixed $\alpha=0.1,0.15,\ldots,1$ from bottom to top (with the same α labelling as in Fig. 4).

the introduction of the vacancy string operator

$$P_0(x) = \left\langle \prod_{y=1}^{x} v_y \right\rangle, \tag{3}$$

which counts the probability of the entire road to the left of $x+1$ being empty. $P_0(L)$ acts as an order parameter, which vanishes in the C and MC phases, but remains nonzero across the entire chain in the ER phase. $P_0(x)$ is always nonzero near the entrance at small x.

The qualitative structure of the phase diagram is now easily understood. In the stationary state, the average current is constant throughout the system, and Eq. (2) implies the identity

$$\alpha\langle v_1\rangle = 1-(1-p)\langle v_L\rangle - pP_0(L). \tag{4}$$

This excludes the C and MC phases from extending into the $p>\alpha$ region of the phase diagram. The identity cannot be satisfied for $p>\alpha$ with $P_0(L)=0$; the right-hand side varies

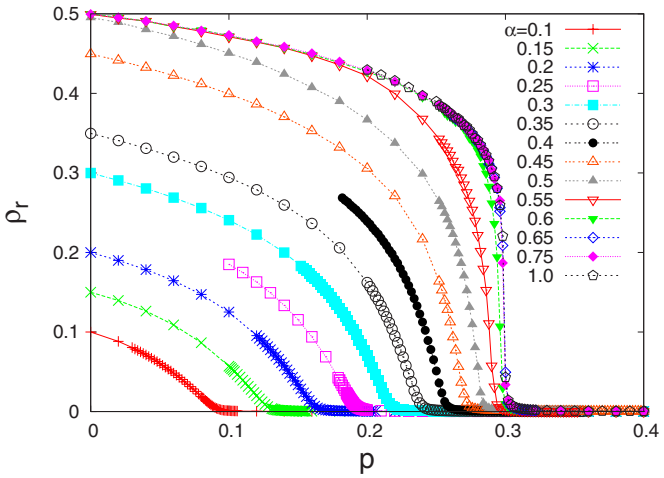

FIG. 4. (Color online) Steady-state bulk road particle density ρ_r versus p at fixed $\alpha=0.1,0.15,\ldots,1.0$ for $L=8000$.

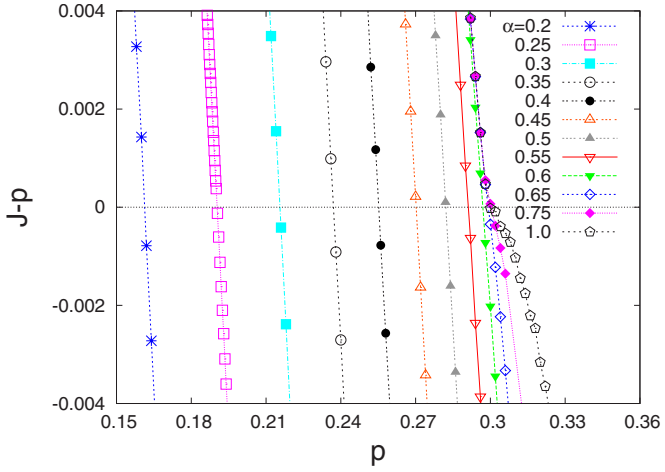

FIG. 5. (Color online) J-p versus p at fixed $\alpha=0.2,0.25,\ldots,1.0$ for $L=8000$. The intersection points with the J-$p=0$ line represent the C-ER and the MC-ER phase transition points.

between p and 1, because $0\leqslant v_L\leqslant 1$, and that is inconsistent with $0\leqslant v_1\leqslant 1$ for $p>\alpha$.

Equation (2) also implies that the current along the entire transition line is equal to $J=p_c(\alpha)$; because at p_c, $\langle v_L\rangle$ is already equal to 1, while $P_0(L)$ is still equal to zero. Our numerical simulations confirm this.

The leveling off of the transition line into a horizontal (constant p) segment is linked to this as well. As a start, we consider MF theory. In the MC phase, where the bulk controls the current, Eq. (1) is then approximated as $J=v_b-(1-p)v_b^2$ where v_b is the vacancy density deep inside the bulk. The maximum current representation of MF theory, $\delta J/\delta v_b=0$, yields, $v_b=1/2r$ and $J=1/4r$, with $r=1-p$. This together with the condition $J(p_c)=p_c$ puts the MC-ER transition line at $p=1/2$.

This is only an upper limit to its true location. The clustering in the MC phase, shown in Fig. 2, is not represented in MF theory. It underestimates the number of nearest-neighbor

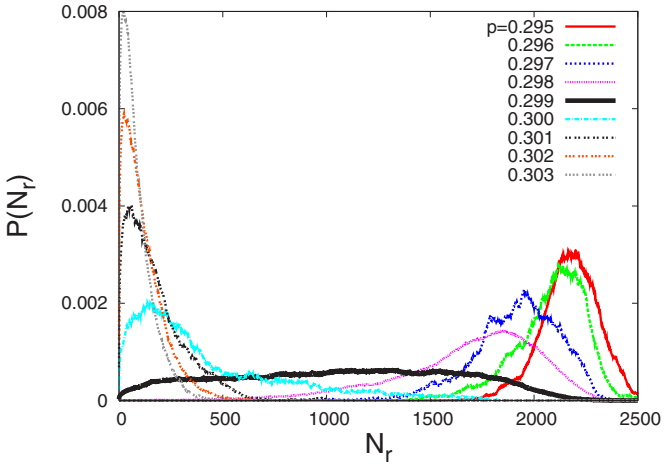

FIG. 6. (Color online) Probability distribution $P(N_r)$ for finding N_r particles on the road, at $\alpha=0.75$ for various $p=0.295,0.296,\ldots,0.303$ (from right to left) at $L=8000$. The MC-ER transition occurs at $p_c\approx 0.299$.

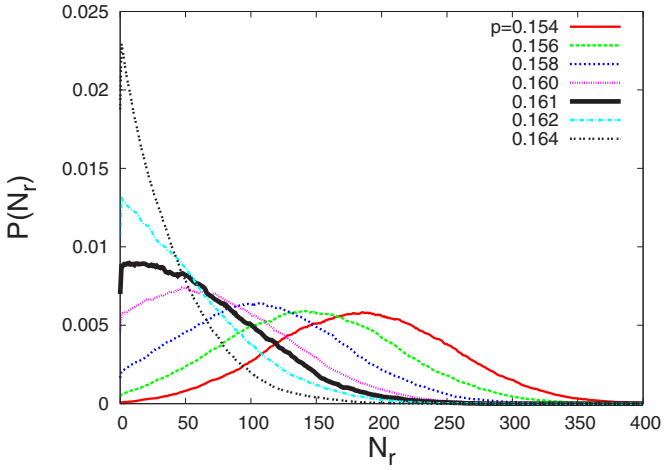

FIG. 7. (Color online) Probability distribution $P(N_r)$ for finding N_r particles on the road, at $\alpha=0.2$ for various $p=0.154, 0.156, \ldots, 0.164$ (from right to left) at $L=8000$. The C-ER transition occurs at $p_c \approx 0.161$.

pairs. These pairs shift the transition line downward [see Eq. (1)]. More advanced versions of MF theory incorporate local correlations but still fail to account for clustering. Instead, we develop in the following section a self-consistent cluster approach. It predicts the correct location of the MC-ER transition line, and, more importantly, it provides insight in the mechanism that makes the MC-ER transition discontinuous.

We note that a closed chain (with periodic boundary conditions) does not include the ER phase due to conservation of the total number of particles and holes in such a setup. A similar model was studied in the context of the mass-conserving coalescence process, the so-called mass-chipping model [20,21] with and without a bias. Implications of our results in this context will be discussed elsewhere [22].

III. FREE CLUSTER ANALYSIS

Adopt the point of view where the C and MC type stationary state configurations are fully clustered, with one distinct "mother cluster" attached to the entry reservoir at small x and many disconnected freely drifting clusters in the bulk. These clusters are meant to be only mesoscopic in size, because true phase separation in terms of macroscopic high-density (clusters) and low-density sections is not realized in this process (see Fig. 2).

Assume the bulk clusters are compact nonfractal mesoscopic objects with average bulk density ρ_c and local average densities ρ_F and ρ_R at the front x_F and rear x_R ends, respectively. The front moves forward by creep (local hops, $x_F \to x_F+1$) and backward by detachment of the front particle by a nonlocal hop to the next cluster, with velocity

$$u_F = \frac{\partial x_F}{\partial t} = (1-p) - p/\rho_F. \tag{5}$$

The rear moves by local forward hops (internal nonlocal hops are suppressed by the high particle density inside the clusters) and by attachment of a new particle due to a nonlocal hop from the free cluster behind it,

$$u_R = \frac{\partial x_R}{\partial t} = (1-\rho_R) - p. \tag{6}$$

The drift velocity u_d of the cluster is associated with its center of mass;

$$u_d = \frac{1}{2}(u_F + u_R) = 1 - p - \frac{1}{2}\rho_R - \frac{1}{2}p/\rho_F. \tag{7}$$

A cluster maintains its integrity only if its internal bulk density ρ_c is stationary. The number of particles in the cluster, N_c, is determined by nonlocal hops at its two ends, and is thus on average constant in time, $\partial N_c/\partial t \simeq -p+p=0$. A stationary internal density ρ_c requires therefore that the average cluster length $\xi=x_F-x_R$ be invariant. Equations (5) and (6) then relate the front and rear densities as

$$\rho_R \rho_F = p. \tag{8}$$

Inserting reasonable values for the densities yield immediately that u_d changes sign as p increases, and does so before the MF estimate of p_c. For example, $\rho_F=1/2$ implies that the drift velocity changes sign at $p_c=1/3$; and also that $\rho_R=2/3$, large enough to validate the cluster concept self-consistently.

This turnabout of the drift velocity of the clusters explains the first-order nature of the MC-ER transition. Any initial configuration decays (after forming clusters) to an empty road for $u_d<0$, because all bulk clusters travel backward and fall back into the entry point reservoir. This change in drift velocity is clearly visible in the density profile time evolutions of Fig. 2.

Emboldened by this success, we dare to push the self-consistent cluster analysis further. We need to relate the above equations to the free cluster current J_c and bulk density ρ_c to obtain a closed set of equations. To determine the free cluster properties throughout the C and MC phases, and also estimate the value of p_c.

Visualize each cluster as a separate conventional ASEP, i.e., the absence of significant numbers of internal nonlocal hopping events due to the high local internal density. In the conventional ASEP the density probability distribution deep inside the bulk is spatially uncorrelated. It is safe to presume the same is true inside the clusters. This yields

$$J_c = (1 - r v_c) v_c, \tag{9}$$

with $r=1-p$. The cluster acts like an individual ASEP with open boundary conditions in a somewhat unusual setup: It has a fluctuating "lattice size" ξ and a fixed injected current p, instead of a fixed lattice size and a fluctuating injection current (controlled by a fugacity like α). The total current inside a cluster is equal to the injection current plus the contribution of the center of mass drift as

$$J_c = p + \rho_c u_d. \tag{10}$$

J_c and ρ_c should not be confused with the global current and density. They only coincide with those at the transition point $u_d=0$. Equation (10) reproduces correctly the exact result that $J=p_c$ at the transition.

Equations (7)–(10) provide still only four conditions between five variables: the cluster current J_c, the drift velocity

u_d, and the rear, bulk, and front densities (ρ_R, ρ_c, and ρ_F). Typically (at a given value for p), a set of possible solutions can be found. Let us parametrize them by their values for J_c. We use the maximal current principle to close the equations and select the correct value of J_c from the set. The justification of this is again based on the conventional ASEP, where the exact matrix method solution as well as the MF approximation have this property [4]. A secondary feature of the conventional ASEP is also preserved, that the stationary state density profile is always uniformly decreasing, $\rho_R \geqslant \rho_c \geqslant \rho_F$.

This procedure leads to two distinct types of free cluster solutions as a function of p: a "front-limited" (F) state (with $\rho_c=\rho_F$) at $p>p_s$; and a "maximum current" (MC) state (with $\delta J/\delta v_c=0$) at $p<p_s$. The crossover takes place at $p_s=\frac{1}{4}(3-\sqrt{5})=0.191$.

The MC free cluster solution at $p<p_s$ resembles very closely and smoothly connects to the $p=0$ global MC state. It has internal vacancy density $v_c=1/2r$, cluster current $J_c=14r$, drift velocity $u_d=r-1/2$, and edge densities $\rho_F=2p$ and $\rho_R=1/2$. However, we cannot take the MC free cluster solution seriously at small p, because the internal cluster density becomes too small for the cluster concept to remain meaningful. Instead, we interpret p_s as marking the onset of crossover toward the nonclustered MC stationary state at $p=0$.

The F solution with $\rho_c=\rho_F$, maximizes the internal current inside the cluster for $p>p_s$. The cluster density is equal to

$$\rho_c = \frac{1}{2(1-p)}(\sqrt{4p-3p^2}-p). \tag{11}$$

The rear density $\rho_R=p/\rho_c$ is larger than $\rho_c=\rho_F$ in the entire interval $p_s<p<p_c$, reflecting a uniformly decreasing density profile (required for internal stability).

These F solutions tell us that inside the MC phase (bulk-in-control phase) of Fig. 1, near p_c, the configurations are clustered and that each of these free clusters is limited and controlled by its front. Inserting $\rho_c=\rho_F$ from Eq. (11) into Eq. (5) yields $u_d=0$ at $p_c=1/3$. This estimate for the first-order transition line is remarkably close to our numerical results, $p_c \simeq 0.30$.

IV. MOTHER CLUSTER ANALYSIS

We now turn our attention to the critical line between the C and ER phases. This transition is dominated by the fluctuations near $x=1$. Therefore, we extend the self-consistent cluster analysis to the mother cluster, i.e., the cluster attached to the entry point reservoir. This analysis explains the scaling properties of the second-order transition, as determined numerically and presented in the following sections.

The mother cluster is presumed to be a mesoscopic object, connected to the entry side reservoir. It governs the bulk current in the C phase, while being controlled itself by the reservoir. The mother cluster acts like a $p=0$ ASEP with a fluctuating front, i.e., with a fluctuating length. The injection current from the reservoir in its rear is equal to $J_c=\alpha v_1$, with $v_x=1-\rho_x$ as before. The bulk density of the mother cluster can be presumed to be uncorrelated again, Eq. (9). The evolution of its front at x_F obeys Eq. (5). An amount p of the current through the cluster flows away at the front of the cluster by nonlocal hops, and the remainder extends the cluster forward:

$$J_c = p + \rho_c u_F = p + \rho_c[(1-p) - p/\rho_F]. \tag{12}$$

This set of equations is still incomplete. It ignores the probability $P_0(x)$ that all sites to the left of a specific site x are empty [see Eq. (1)]. In the free cluster analysis this played no role [$P_0(x)=0$] because another particle can always be found to the left of the free cluster as long as the mother cluster exists and remains mesoscopic. The mother cluster current is very sensitive to the density profile near the reservoir, and thus to $P_0(x)$.

The mother cluster density profile can be presumed (self-consistently) to be sufficiently uniform that we can apply mean-field theory internally,

$$v_{x+1} = J_c/[1 - rv_x - pP_0(x)], \tag{13}$$

$$P_0(x) = v_x P_0(x-1). \tag{14}$$

Compare this with Eq. (1). MF theory for the conventional ASEP gives erroneous power-law and exponential density profile tails. Similarly, the following analysis can be at best only qualitatively correct.

Solutions are found by solving the above equations iteratively and by finding the value of J_c that satisfies the boundary conditions at both the rear and front. It is important to realize that the solution is unique for "finite" cluster lengths ξ_c. The mother clusters are finite in length, but we analyze them as if they are mesoscopic and effectively infinitely long. For infinite cluster lengths, the equations typically allow a range of J_c with possible solutions. The maximum current solution is the correct one, because it coincides with the $\xi_c \to \infty$ limit of the unique finite length solution.

At $\xi_c=\infty$, the construction of a solution involves the matching of two iteration processes: the forward iteration, $x \to x+1$, starting from the rear of the cluster and the backward iteration, $x \to x-1$, starting from the front of the cluster. It is useful to sketch briefly some of the details of this. The iteration process has two bulk densities as possible fixed points, determined by the roots of the quadratic equation $J_c=v_c(1-rv_c)$ (using that $P_0 \to 0$ in the bulk of the mother cluster). The low-density fixed point $v_c^{(l)}$ is unstable and the high-density fixed point $v_c^{(h)}$ is stable in the forward iteration process. They reverse roles in the backward iteration process.

For a given value of J_c, the forward iteration process starts at site $x=1$ with density $v_1=J_c/\alpha$, and typically iterates toward $v_c^{(h)}$ (see Fig. 8). The backward iteration process starts at site $x=x_F$ with density v_F prescribed by Eq. (12), and typically converges toward $v_c^{(l)}$. Those solutions do not match, unless the current is raised to the value where the two fixed points coincide. This matching is equivalent to (and the origin of) the maximal current principle. This type of solution, where the two fixed points merge, applies to the bulk-controlled MC state. It exists when the starting densities of

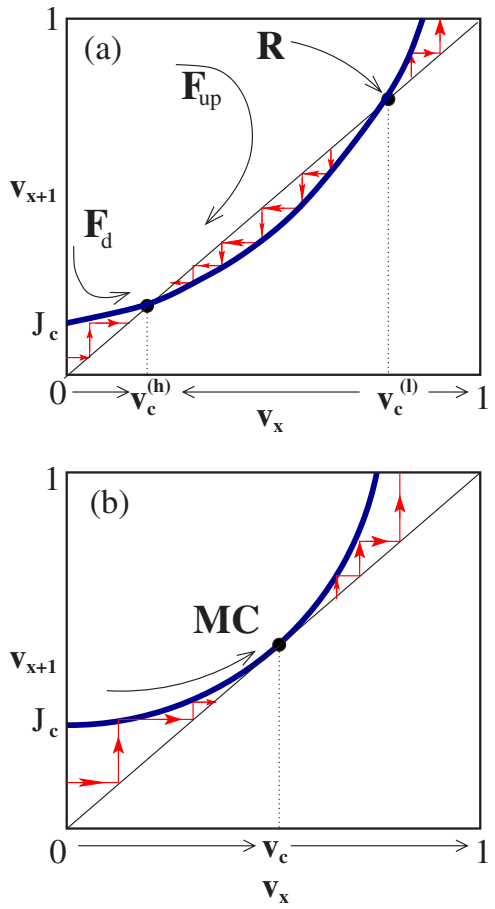

FIG. 8. (Color online) Forward iteration processes.

the forward and backward iteration processes are located inside the attraction domain of the $v_c^{(h)}$ and $v_c^{(l)}$ fixed points, respectively.

This fails in the front- and rear-controlled F- and R-type states. In the F states, the starting point of the backward iteration process, the value v_F, crosses over to the unstable side $v_F < v_c^{(h)}$ of the $v_c^{(h)}$ fixed point, while we raise the current. In that case J_c must be chosen such that those two densities match, $v_F = v_c^{(h)}$. The density profile at the front is thus flat. The rear profile is typically able to iterate forward toward this fixed point $v_c^{(h)}$, and thus match the backward iteration. (This solution still maximizes the current, in the boundary-limited sense.)

In the rear-controlled (R) states, the roles of the forward and backward iteration processes are reversed, i.e., the forward iteration process crosses over to the wrong side of the $v_c^{(l)}$ fixed point. This requires more care than the F state, because the initial value $v_1 = J/\alpha$ needs to be iterated forward into the region $x \simeq l_p$ where $P_0(x)$ becomes negligible, before it becomes clear where this profile "lands" compared to the low-density fixed point $v_c^{(l)}$. The latter is the reason why we need to bother with the iteration process for the mother cluster, while for the free clusters it suffices to write down the boundary and bulk conditions, and use the maximal current principle formulation of the matching process.

Figure 9 shows the mother cluster states as a function of α and p. The MC (bulk-controlled) and F (front-controlled)

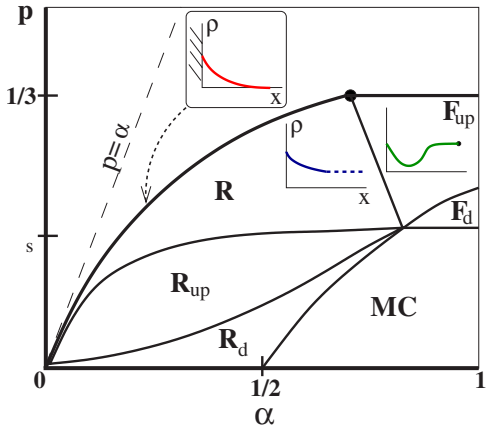

FIG. 9. (Color online) Mother cluster states in the α-p phase diagram.

states are basically identical to the free cluster states discussed in the earlier section. This confirms the stability of the MC clustered phase at large α. In these states the front or bulk of the mother cluster is in control, setting J_c, and at the rear the reservoir is able to supply the requested current without letting the mother cluster detach. The F state can be divided into two states, F up and F down, distinguishing between whether the forward iteration process approaches $v_c^{(h)}$ from below or above (see Figs. 8 and 9). In the free cluster analysis only F down is present. Due to the presence of $P_0(x)$, the mother cluster is not required to be uniformly decreasing any more.

These F and MC solutions describe mesoscopic mother clusters. The growth velocity (drift velocity of the front) u_F is positive. Strictly speaking the mother cluster could keep growing until it fills the entire chain, but that would lead to the uniform MF-type nonclustered state along the entire chain. In reality, density fluctuations make the mother cluster break apart regularly, emitting free clusters.

The transition into the R states at small α takes place when the front (F state) or bulk (MC state) imposed value of J_c can no longer be satisfied at small x. From there on, the rear takes over as the limiting factor, and the front end of the profile is required to follow instead. This is the origin of the starvation process responsible for the second-order transition line.

The mother cluster front can only follow the rear at small p, denoted in Fig. 9 as the R-up and R-down states. The current J_c must be tuned such that the forward iteration process lands exactly onto the low-density fixed point $v_c^{(l)}$. In the R-up and R-down states, the backward iteration process, starts at a v_F inside the attraction basin of the low-density fixed point, and therefore the backward iteration process is able to converge.

The R-up state has an increasing density profile in the front, where $P_0 = 0$, and is therefore dynamically unstable. Moreover, the bulk densities in both the R-up and R-down states are very small, just as in the MC state, and self-inconsistent with the cluster concept. The mother cluster density profile starts high at $x = 1$, but decays to the small unstable fixed point value beyond $x = l_p$. Such clusters must be unstable to internal clustering fluctuations and break up regularly into a small l_p-sized object.

Everywhere near the second-order transition line, in the area marked as R in Fig. 9, the backward iteration process fails because v_F starts at a $v_F < v_c^{(h)}$ outside the attraction basin of $v_c^{(l)}$. The forward and backward iterations can not be matched anymore. A true R-type mother cluster solution seizes to exist. The front of the mother cluster can not be in a locally stable stationary type forward creeping state anymore.

This inability to construct a stable R cluster front near the second-order transition line in Fig. 1, leaves no other options than to toss out the mother cluster front conditions, Eq. (12), and redefine the mother cluster as a quasistationary R-type object (typically short, except very close to the second-order transition line) defined by the half-space forward iteration process only, with J_c the precise value of the cluster current that let $v_1 = \alpha / J_c$ iterate into $v_c^{(l)}$. The mother cluster size is set by the length scale l_p where $P_0(x) \to 0$ and the density becomes small. l_p is now the onset of a turbulent low-density region where the formation of new free clusters takes place continuously without any "local stationary state order" or stability.

Next, we face the problem that we lost our (maximum current) justification for why J_c must settle on that special value where the forward iteration process converges into the unstable fixed point. Nevertheless, it is arguably the dynamically stable choice in the following sense. Consider the half-space solutions with smaller values of J_c. Their forward iteration process converges into the stable high-density fixed point. Those clusters would have a pronounced dip in their density profile near l_p (when the iteration process comes near the $v_c^{(l)}$ fixed point) before increasing towards the large density value of the $v_c^{(h)}$ fixed point. Such structures are unstable and tend to shrink. They resemble mother clusters in the process of pinching off a free cluster. The breaking-up event shrinks the mother cluster toward l_p. Moreover, the breakup also increases the current of the combined two objects. Half-space solutions with values of J_c larger than the special choice make the iteration process crash almost immediately through zero density, and can be interpreted as representing very short mother clusters. Those are also unstable and tend to grow. The empty space in front of such a short cluster can carry away still only a current of order p, while J_c has increased. Moreover, it is less successful in breaking up because $P_0(x)$ is not small at its front, and therefore the free cluster immediately in front of it is subject to a fluctuating injection current, larger on average than p, and thus with a significantly smaller or even negative drift velocity.

The C-MC phase boundary is represented in the mother cluster analysis as the threshold (see Fig. 9), between the R states and the MC and F states. This reproduces the true location (from our numerical simulations) not too well. It has a kink instead of being smooth. The reason for this is likely that the mother cluster is very short in the R states and badly approximated by the mesoscopic description.

The C-ER critical line is represented in the mother cluster analysis as the line where the R-state solution iterates to zero density. This estimate virtually coincides with the true location determined from our numerical simulations. This remarkable accuracy is likely linked to the fact that the mother cluster length, of order l_p, diverges at the transition, and the mesoscopic approach becomes valid.

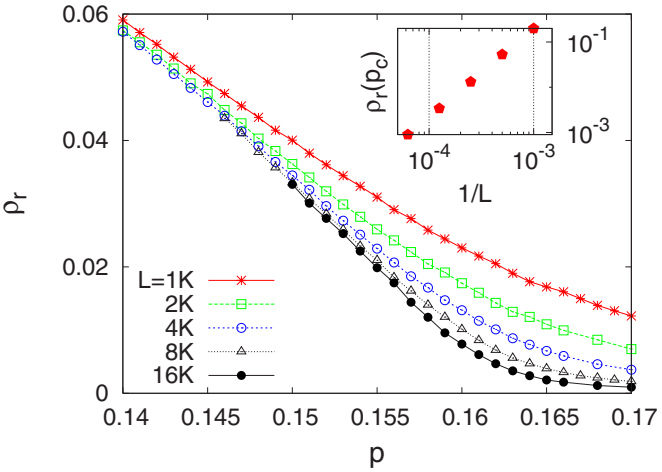

FIG. 10. (Color online) Road density ρ_r versus p at $\alpha = 0.2$ for various L. The inset illustrates the finite-size behavior of ρ_r at the C-ER transition point in a log-log plot.

The crossover from the horizontal first-order segment of the transition line to the curved second-order part represents a critical end point. It is located at exactly $p_c = 1/3$ and $\alpha = 2/3$ in this analysis, and is also close to the true location. Our numerical simulations locate it at $p_c \simeq 0.300(2)$ and $\alpha \simeq 0.64(1)$. The scaling properties of the critical end point appear numerically not special, and consistent with the notion, emerging from the cluster analysis, that the origins of the first- and second-order transitions (starvation versus drift-velocity turnabout) are distinct and unrelated. Their scaling behaviors are thus simply superimposed onto each other at the critical end point.

Within our numerical accuracy this critical end point coincides with the end point of the C-MC boundary. There is no *a priori* reason to expect this coincidence, but in the mother cluster approach it arises naturally.

V. NUMERICAL RESULTS AT CRITICALITY

In our numerical simulations, we average over 10^4–10^5 independent runs up to $t = 10^5$ Monte Carlo steps for nonstationary state features. For the stationary state properties we simulate system sizes $L = 500 \times 2^n$ with $n = 1, 2, \ldots, 5$ and discard all data before $t \simeq L^2$ or more, to allow the system to reach the stationary state. We collect data up to $t = 10^8$–10^9 Monte Carlo steps and average over 10–200 independent runs. We monitor the road density $\rho_r = \langle n_r \rangle$ $(n_r = N_r / L)$; the density fluctuations $\chi_2 = L(\langle n_r^2 \rangle - \langle n_r \rangle^2)$; the Binder cumulant $U_4 = 1 - \langle n_r^4 \rangle / (3 \langle n_r^2 \rangle^2)$; and the current J. The results are shown in Figs. 10 and 11.

The scaling properties of the C-ER transition are determined numerically, along several cuts though the transition line. It suffices to present here the details along one representative example, i.e., only the $\alpha = 0.2$ line. The critical point p_c along this line can be determined by standard methods, from the so-called crossing points or the maximum

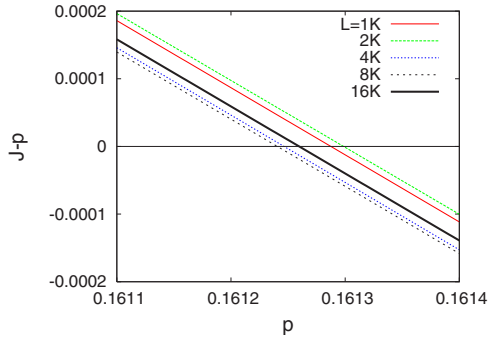

FIG. 11. (Color online) Details of J-p versus p as a function of p at $\alpha=0.2$ for various L show that finite-size corrections are very small and $J(p_c)=p_c=0.161\,25(5)$. Compare with Fig. 5.

points in χ_2 as well as the crossing points in U_4. From these we estimate $p_c=0.161(1)$. As mentioned before, the current (see Fig. 11) must be equal, $J=p$, at the transition line. This is very well satisfied compared to the above estimate for p_c. Turning this around, requiring $J(p_c)=p_c$, improves the estimate to $p_c=0.161\,25(5)$.

The road density ρ_r vanishes on approach of the transition point p_c from below in the thermodynamic limit, as $\rho_r \sim \Delta^\beta$ with $\Delta=p_c-p$. The density fluctuation χ_2 diverges at p_c from below as $\chi_2 \sim \Delta^{-\gamma}$ but becomes zero in the ER phase ($p > p_c$). The Binder cumulant U_4 converges to 2/3 in the C phase (consistent with a Gaussian distribution) and to -1 in the ER phase (indicating an exponential distribution). U_4 converges very fast, while $\chi_2^{(m)}$ shows strong finite-size effects.

The values of the critical exponents follow by exploiting conventional finite-size scaling theory,

$$\rho_r = L^{-\beta/\nu} f(\Delta L^{1/\nu}),$$

$$\chi_2 = L^{\gamma/\nu} g(\Delta L^{1/\nu}),$$

$$U_4 = h(\Delta L^{1/\nu}), \tag{15}$$

where ν is the correlation length exponent and f, g, and h are scaling functions. Elementary scaling laws yield hyperscaling relations such as $(2\beta+\gamma)/\nu=1$.

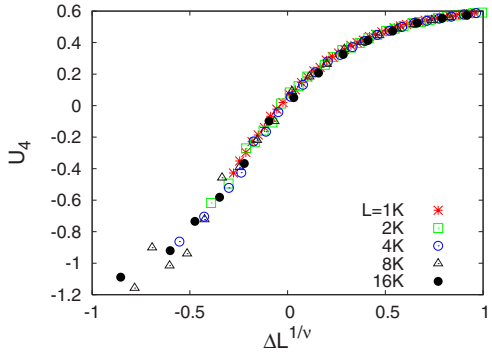

FIG. 12. (Color online) Scaling collapse of the Binder cumulants at $\alpha=0.2$ with $p_c=0.161\,25$ and $1/\nu=0.50$.

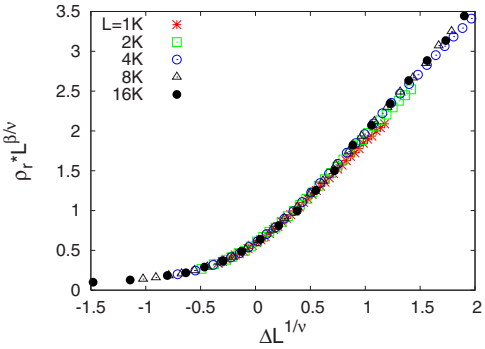

FIG. 13. (Color online) Scaling collapse of ρ_r at $\alpha=0.2$ with $p_c=0.161\,25$, $\beta/\nu=0.48$, and $1/\nu=0.53$.

U_4 shows the least finite-size effects. We estimate the value of ν by collapsing the U_4 data (see Fig. 12) as $1/\nu=0.50(2)$. Collapsing the road density data yields (see Fig. 13) $\beta/\nu=0.48(2)$ and $1/\nu=0.53(3)$. By plotting the maximum value of χ against L, we can estimate the value of γ/ν. A simple power-law fitting yields $\gamma/\nu=0.17(3)$, but the data are also consistent with a logarithmic fit, i.e., $\chi_2^{(m)} \sim \ln L$ (see Fig. 14). Hyperscaling is satisfied only when this logarithmic divergence is correct, so we are inclined to put more weight on the logarithmic fitting.

The value of the Binder cumulant $U_4(p_c)$ is expected to be universal at the transition. Our numerical estimate $U_4(p_c)=0.08(3)$ is very close to zero, which may reflect the half-Gaussian-like shape of $P(N_r,L)$ at criticality (see Fig. 7).

VI. MOTHER AND FREE CLUSTER SEPARATION

The numerical data point to rather simple values of the critical exponents at the C-ER transition, $\beta=1$ and $\nu=2$. The R-state mother cluster properties explain why the scaling is that simple. The first and most crucial observation is the lack of any feature in the current $J(p,\alpha)$ across the critical line in our numerical data, Figs. 5 and 11. The global current appears to be analytic, and totally unaffected by the presence of the C-ER transition, moving linearly through the critical value $J=p$, as $J-p \simeq A(p-p_c)$.

The mother cluster sets the global average current. Its offspring, the free clusters, cannot influence this, unable to

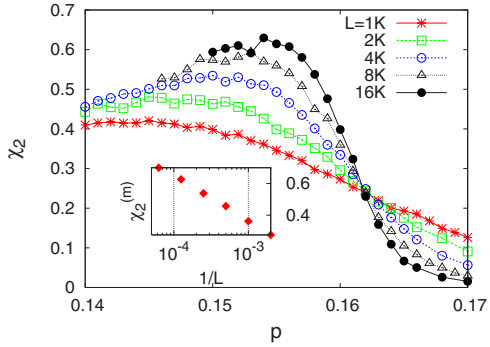

FIG. 14. (Color online) Density fluctuations χ_2 versus p at $\alpha=0.2$ for various L. The inset shows the finite-size behavior of the maximum values $\chi_2^{(m)}$ in a semilogarithmic plot.

communicate in the backward direction, being distinct objects with positive drift velocity. The mother cluster is an independently fluctuating object, and the rest of the road is slaved to it. At the C-ER transition, the mother becomes unable to create free clusters at a sufficient rate to sustain a nonzero average bulk density ρ_c, but is itself unaffected by what is going on in the bulk.

The global average current $J(\alpha,p)$ is analytic across the C-ER transition, because the mother cluster current is analytic, and the average bulk current is equal to it, because (on average) the mother cluster remains attached to the reservoir, and (on average) it does not grow in length (due to the breaking off of free clusters).

The linear vanishing of the bulk density with exponent $\beta=1$ is a direct consequence of this analyticity of $J(\alpha,p)$. They are related by the simple equation

$$J(\alpha,p) = p(1-\rho_r) + (p + \rho_c^{(f)} u_d^{(f)})\rho_r, \tag{16}$$

$$\rho_r = \frac{J-p}{\rho_c^{(f)} u_d^{(f)}}, \tag{17}$$

with $\rho_c^{(f)}$ the internal free cluster bulk density and $u_d^{(f)}$ the drift velocity [see also Eq. (10)]. Consider a specific bond. The first term on the right-hand side of Eq. (16) represents the current through this bond from isolated nonlocally hopping particles when this bond is not part of a free cluster. The second term is the current through the bond when it is part of a free cluster. The probability for the bond to be part of a free cluster is equal to ρ_r. The free cluster parameters $\rho_c^{(f)}$ and $u_d^{(f)}$ are analytic functions of p only and are set self-consistently by the free cluster equations. All functions on the right-hand side of Eq. (17) are analytic; therefore the bulk density vanishes linearly, with $\beta=1$.

The C-ER transition is a bulk phenomenon induced by the mother cluster. It lacks therefore independent critical bulk fluctuations. This explains why $\nu=2$. The free clusters generating breakups in the turbulent region near $x=l_p$ behave like random uncorrelated events; i.e., the fluctuations in the number of particles injected by the mother cluster into the bulk behave like uncorrelated noise. In the C phase, those fluctuations are screened and absorbed by the presence and formation of free clusters. On approach to the C-ER transition, free clusters become rare and at the transition they vanish altogether. There, the random breakup fluctuations travel like a pattern across the chain. The time of flight is proportional to the system size. Therefore, the bulk density represents (biased) random noise averaged over a time proportional to L, and thus scales as $\rho_r \sim L^{-1/2}$ at the C-ER transition.

Two more variables in our numerical data express and confirm the same uncorrelated fluctuations. At the C-ER transition, the density profile (no figure included) decays to zero smoothly near the reservoir, as a power law, $\rho_r(x) \sim x^{-\delta_R}$ with $\delta_R \approx 1/2$, consistent with random noise. In the C phase, the distribution of the number of particles on the road, $P(N_r)$, is a Gaussian centered around the bulk density ρ_r. Toward the C-ER transition, the maximum shifts toward $N_r \approx O(1)$ and at the transition decays as a half Gaussian (see Fig. 7) consistent with uncorrelated noise. In the ER phase, $\rho_r(x)$ and $P(N_r)$ decay exponentially.

VII. CONCLUSIONS

In this paper, we studied how the inclusion of nonlocal hopping events affects the stationary state of the ASEP. Clusters develop, but mesoscopic ones. There is no macroscopic queuing transition. Instead, there is a phase transition toward an empty-road phase, which is first order from the MC clustered phase (where the bulk is in control) and second order from the C-type clustered phase (where the entry reservoir controls the stationary state). The first-order MC-ER transition is induced by a reversal of the group velocity of the free clusters. The C-ER transition has rather simple scaling properties, reflecting the mother cluster properties near the entry reservoir and that the bulk (free clusters) do not interact back on the mother cluster.

One of the remaining issues is the nature of the dynamic scaling. Generically, fluctuations in the stationary state broaden in time as $l \sim t^{1/z}$. The dynamic scaling in the clustered C and MC phases, is to be expected to remain in the Kardor-Parisi-Zhang universality class, with $z=3/2$. Within each cluster length scale we expect $z=3/2$ because each cluster acts like a simple ASEP in its own right. At larger length scales, the process resembles a driven zero-range process with a preferred direction and nonzero group velocity, which should also have $z=3/2$ scaling. In our simulations, we did not focus on the dynamic scaling properties of the C ad MC phases, but exploratory numerical results for z are consistent with $z=3/2$. The dynamic scaling at the C-ER transition is expected to remain simple as well because that transition does not involve novel intrinsic bulk fluctuations.

Clustering and its ramifications are surely the main message of our study. The conventional ASEP has a uniform stationary state with rather trivial scaling properties, but is unstable toward clustering and queuing. Such clustered states, even when involving only mesoscopic clusters, communicate badly with each other, and it is hard for them to develop to other types of fluctuations. Phase transitions, induced and controlled by those same clusters, therefore have typically rather simple scaling properties, as at the C-ER and MC-ER phase boundaries in our process.

It will be interesting to test our self-consistent cluster approximations on other processes with clustering in cases where the drift velocity of the clusters is nonzero; for example, a variant of the two-species process of Arndt *et al.* [8] with different numbers of oppositely moving particles.

ACKNOWLEDGMENTS

We wish to thank D. Mukamel, G. M. Schütz, and R. P. K. Zia for useful discussions. This work was supported by the National Science Foundation under Grant No. DMR-0341341 and by the BK21 project.

[1] B. Schmittmann and R. K. P. Zia, in *Phase Transitions and Critical Phenomena*, edited by C. Domb and J. Lebowitz (Academic, London, 1995), Vol. 17.

[2] G. M. Schültz, in *Phase Transitions and Critical Phenomena*, edited by C. Domb and J. Lebowitz (Academic, New York, 2001), Vol. 19.

[3] J. T. MacDonald, J. H. Gibbs, and A. C. Pipkin, Biopolymers **6**, 1 (1968); J. T. MacDonald and J. H. Gibbs, *ibid.* **7**, 707 (1969).

[4] B. Derrida, M. R. Evans, V. Hakim, and V. Pasquier, J. Phys. A **26**, 1493 (1993); B. Derrida, E. Domany, and D. Mukamel, J. Stat. Phys. **69**, 667 (1992).

[5] M. Ha and M. den Nijs, Phys. Rev. E **66**, 036118 (2002).

[6] M. Myllys, J. Maunuksela, J. Merikoski, J. Timonen, V. K. Horváth, M. Ha, and M. den Nijs, Phys. Rev. E **68**, 051103 (2003).

[7] M. Ha, J. Timonen, and M. den Nijs, Phys. Rev. E **68**, 056122 (2003). For more details, see also M. Ha, Ph.D. thesis, University of Washington, 2003 (unpublished).

[8] P. F. Arndt, T. Heinzel, and V. Rittenberg, J. Phys. A **31**, L45 (1998); J. Stat. Phys. **97**, 1 (1999).

[9] N. Rajawsky, T. Sasamoto, and E. R. Speer, Physica A **279**, 123 (2000); T. Sasamoto and D. Zagier, J. Phys. A **34**, 5033 (2001).

[10] Y. Kafri, E. Levine, D. Mukamel, G. M. Schütz, and J. Török, Phys. Rev. Lett. **89**, 035702 (2002); Y. Kafri, E. Levine, D. Mukamel, and J. Török, J. Phys. A **35**, L459 (2002).

[11] F. Spitzer, Adv. Math. **5**, 246 (1970).

[12] *Traffic and Granular Flow '97*, edited by M. Schrenckenberg and D. E. Wolf (Springer-Verlag, Singapore, 1998).

[13] P. Biswas, A. Majumdar, A. Mehta, and J. K. Bhattacharjee, Phys. Rev. E **58**, 1266 (1998).

[14] R. Lahiri and S. Ramaswamy, Phys. Rev. Lett. **79**, 1150 (1997).

[15] M. A. Rutgers, J.-Z. Xue, E. Herbolzheimer, W. B. Russel, and P. M. Chaikin, Phys. Rev. E **51**, 4674 (1995); S. E. Paulin and B. J. Ackerson, Phys. Rev. Lett. **64**, 2663 (1990).

[16] P. Král and M. Shapiro, Phys. Rev. Lett. **86**, 131 (2001); L. A. Clark, G. T. Ye, and R. Q. Snurr, *ibid.* **84**, 2893 (2000).

[17] B. Drossel and M. Kardar, Phys. Rev. Lett. **85**, 614 (2000).

[18] M. E. Fisher and A. B. Kolomeisky, Physica A **274**, 241 (1999); T. Harms and R. Lipowsky, Phys. Rev. Lett. **79**, 2895 (1997); F. Jülicher and J. Prost, *ibid.* **78**, 4510 (1997).

[19] T. Nattermann, Phys. Rev. Lett. **64**, 2454 (1990); M. V. Feigel'man, V. B. Geshkenbein, A. I. Larkin, and V. M. Vinokur, *ibid.* **63**, 2303 (1989); D. R. Nelson, *ibid.* **60**, 1973 (1988).

[20] R. Rajesh and S. N. Majumdar, Phys. Rev. E **63**, 036114 (2001); S. N. Majumdar, S. Krishnamurthy, and M. Barma, J. Stat. Phys. **99**, 1 (2000); Phys. Rev. Lett. **81**, 3691 (1998).

[21] R. Rajesh and S. Krishnamurthy, Phys. Rev. E **66**, 046132 (2002).

[22] M. Ha, A. Nagar, and H. Park (unpublished).